

Article

Study on the Influence of Perforating Parameters on the Flow Rate and Stress Distribution of Multi-Fracture Competitive Propagation

Xing Zhao ^{1,2,†}, Jin Zhao ^{3,4,*,†}, Hehua Wang ² and Yuandong Liu ⁵¹ China Zhenhua Oil Company Limited, Beijing 100031, China² China & Chengdu North Petroleum Exploration and Development Technology Co., Ltd., Chengdu 610501, China; wanghehua@zhenhuaoil.com³ School of Mechanical Engineering, Yangtze University, Jingzhou 434023, China⁴ State Key Laboratory of Oil and Gas Reservoir Geology and Exploitation, Southwest Petroleum University, Chengdu 610500, China⁵ China Petroleum Technology and Development Company, Beijing 100028, China

* Correspondence: zhaojin@yangtzeu.edu.cn

† These authors contributed equally to this work.

Abstract: It is of great significance to investigate the flow rate and stress distribution of multi-fracture propagation for the optimization of perforation parameters and fracture parameters. Considering the coupling of rock deformation, fracture direction and fluid flow in multi-fracture scenarios, a mathematical model and solution program for the flow and stress distribution of multiple fractures are established, and the analytical model is used for comparison and verification. The effects of perforation cluster number, cluster spacing, perforation diameter on fracture extension trajectory, fracture width, flow rate of each fracture and stress field are studied by the model. The results show that, as the number of perforating clusters increases, the inner fracture is inhibited more severely with less width, length and flow distribution, as well as lower bottom hole pressure. With the increase in cluster spacing, the stress interference between whole fractures is weakened and the flow distribution of the inner fracture is increased with lower bottom hole pressure. With the decrease in perforation diameter, the inhibition effect of inside fractures is weakened, while the inhibition effect of outside fractures, the flow distribution of inside fractures and the bottom hole pressure are increased. The uniform propagation of multiple fractures can be promoted by decreasing the perforation clusters' number and perforation diameter or increasing fracture spacing.

Keywords: displacement discontinuity method; multi-cluster perforation; flow distribution; stress interference; fluid–solid coupling



Citation: Zhao, X.; Zhao, J.; Wang, H.; Liu, Y. Study on the Influence of Perforating Parameters on the Flow Rate and Stress Distribution of Multi-Fracture Competitive Propagation. *Processes* **2024**, *12*, 839. <https://doi.org/10.3390/pr12040839>

Academic Editors: Hadi Jabbari and Vamegh Rasouli

Received: 30 March 2024

Revised: 16 April 2024

Accepted: 17 April 2024

Published: 21 April 2024



Copyright: © 2024 by the authors. Licensee MDPI, Basel, Switzerland. This article is an open access article distributed under the terms and conditions of the Creative Commons Attribution (CC BY) license (<https://creativecommons.org/licenses/by/4.0/>).

1. Introduction

With the carbon neutrality commitments presented by various responsible countries, there will be a notable transition in the global energy paradigm, moving away from the predominance of fossil fuels toward a greater reliance on non-fossil energy sources over the coming decades. As natural gas generates the least carbon emissions among the fossil energies, it may play an increasingly significant role during the carbon neutrality process. Especially for the coalbed methane, shale gas resource due to its huge reserves, high calorific value and low carbon emission intensity [1–3]. However, owing to the low porosity and permeability of the reservoir and the short effective percolation distance, it is necessary to use the horizontal well volumetric fracturing technology to produce a large induced fracture network, known as stimulated reservoir volume [4–8]. In this process, multiple initiation points can be formed near the wellbore, and multiple fractures expand simultaneously [9–12]. However, distributed optical fiber temperature measurement (DTS) and distributed acoustic sensing (DAS) data from the field indicate that a small number

of fractures could absorb a large amount of fluid and proppant, resulting in non-uniform competitive fracture expansion [13–16].

During the multi-crack competitive propagation process, fracture morphology and flow distribution will change, which will restrict the migration of proppant in the fracture, and ultimately affect oil and gas production [17]. How to reduce the non-uniform fracture propagation, make the amount of fluid and proppant in the fracture evenly distributed and maximize supporting fracture volume has become the focus of attention in the optimization of fracturing treatment design. Many scholars have investigated the mechanism of multi-crack propagation. At present, the displacement discontinuity method (DDM), extended finite element (FEM), discrete element, phase field method and meshless method are the mainstream methods to research the simultaneous propagation of multiple cracks [18–29]. Weng and Hui applied the complex fracture model to investigate fluid diffusion pathways to reactivate pre-existing faults in unconventional reservoirs [30,31]. Crouch and Starfield were the first to propose the displacement discontinuity method (DDM), which has been widely used by many scholars in 2D and 3D hydraulic fracturing simulation, as well as multi-fracture simultaneous expansion simulation [32–34]. Wu et al. used this method to study the propagation of multiple cracks [35,36]. Zhang and Kresse et al. utilized the DDM to simulate the expansion of complex fracture networks [30,31,37–39].

Gordeliy and Peirce developed an implicit level set method based on the fracture tip behavioral mechanics theory [40,41]. Mohammadnejad and Khoei used the XFEM to study the influence of rock mechanics parameters and fracturing parameters on fracture morphology and reservoir pore pressure [42]. Shimizu et al. used the DDM to study the effects of fluid viscosity and particle size distribution on HF cracking initiation and propagation based on the cemented particle model (BPM) [43,44]. Zhang Fengshou et al. simulated the coupling behavior between HF and NF based on the mixed discrete continuum method [45–50]. Chen established the model of fracture turning during propagation based on the theory of fracture mechanics [51]. Zhao used the DDM and extended finite element method to study the stress distribution of multiple cracks [52,53]. Zhang et al. investigated the effect of hole erosion on fracture propagation using downhole perforation imaging data [54]. Zeng proposed a model of multi-fracture growth morphology considering the effect of induced stress [55]. Ouchi used the finite element method to study the effect of fracture propagation on conductivity [56].

However, the mechanism of multi-cluster perforation parameters on the dynamic propagation flow control and stress interference of multi-fracture is still unclear, and how to determine the multi-cluster perforation parameters is still the core problem faced by horizontal well staging fracturing. Therefore, the multi-fracture expansion fluid–solid coupling model is established and validated by the analytical model in this paper. The model takes into account the coupling effect among induced stress, rock deformation, fracture turning and propagation as well as fluid pressure. By utilizing field data, the model reveals the impact of the number of perforation clusters, cluster spacing and perforation hole diameter on both flow distribution and stress distribution. Furthermore, the model also considers how these factors influence each other.

2. Mathematical Mode

The multi-fracture propagation model is an important tool for optimizing multi-fracture geometry and multi-cluster perforating parameters. However, fracture propagation involves many processes such as rock deformation, fracture propagation and fluid flow, and each process affects the other. To simplify those processes, the following assumptions are made:

- (1) The deformation of rock conforms to linear elasticity;
- (2) The height of extending fracture and formation temperature is constant;
- (3) The fracturing fluid flows in one dimension in the fracture with fluid leakage.

For the above assumptions, the mathematical model of nonplanar fracture propagation is established.

2.1. Mode of Rock Deformation

Crouch developed the displacement discontinuity method (DDM), a special boundary element method to describe the rock deformation caused by the fracture opening or shearing in the infinite elastic medium. The fracture is divided into many small fracture elements, and the deformation equation of each crack element can be expressed as follows [57]:

$$\begin{cases} \sigma_s^r(x, y) = \sum_{j=1}^N \int_0^L [G_{11}(x, y, \xi)w(\xi) + G_{12}(x, y, \xi)D_v(\xi)]d\xi \\ p_o(x, y) - \sigma_y^r(x, y) = \sum_{j=1}^N \int_0^L [G_{21}(x, y, \xi)w(\xi) + G_{22}(x, y, \xi)D_v(\xi)]d\xi \end{cases} \quad (1)$$

where σ_s^r, σ_y^r is the remote shear stress and normal stress, Pa; D_v is the shear displacement of fracture element, m; w is the normal displacement of fracture element, m; L is fracture length, m; N is the number of fracture elements; p_o is the injection pressure, Pa; $G_{11}, G_{12}, G_{21}, G_{22}$ are elastic coefficients of fracture elements.

2.2. Mode of Fracture Turning and Propagating

Due to the combined effect of tensile stress and shear stress, two types of cracks will occur: opening cracks (opening mode) and sliding cracks (sliding mode), which will lead to a change in the direction of fracture propagation. The propagation and turning of fractures will be affected by the stress intensity factor of the tip fracture, and the Mode I and Mode II stress intensity factors can be calculated as follows [36]:

$$\begin{cases} K_I = 0.806 \frac{D_{t-n}E}{4(1-\nu^2)} \frac{\sqrt{\pi}}{\sqrt{a_t}} \\ K_{II} = 0.806 \frac{D_{t-s}E}{4(1-\nu^2)} \frac{\sqrt{\pi}}{\sqrt{a_t}} \end{cases} \quad (2)$$

where K_I, K_{II} is the opening mode and shearing mode stress intensity factor, $\text{MPa}\cdot\text{m}^{0.5}$; D_{t-n} is the normal displacement of the crack tip element, m; D_{t-s} is tangential displacement of crack tip element, m; E is Young's modulus of the rock, MPa; ν is the rock's Poisson's ratio; a_t is the tip fracture element length, m.

The equivalent stress intensity factor is determined as [36]

$$K_e = \frac{1}{2} \cos \frac{\theta_0}{2} [K_I(1 + \cos \theta_0) - 3K_{II} \sin \theta_0] \quad (3)$$

When the stress intensity factor reaches the rock toughness K_c , the fracture extends and the failure criterion is as follows [14]:

$$K_e \geq K_c \quad (4)$$

where K_e is the equivalent stress intensity factor; K_c is the rock toughness.

During the process of multiple crack synchronous extension, the velocity of crack tip extension is influenced by the crack tip stress intensity factor and fracture toughness. The extension velocity of each fracture follows Charles power law [8]:

$$a_i = \begin{cases} a \frac{K_{e,i} - K_c}{\max(K_{e,i}) - K_c}, K_{e,i} > K_c \\ 0, K_{e,i} \leq K_c \end{cases} \quad (5)$$

where a_i is the i th fracture element length, m; $K_{e,i}$ is the equivalent stress intensity factor of i th fracture element, $\text{MPa}\cdot\text{m}^{0.5}$.

In addition, crack tip deviation can occur as a result of stress interference. The deviation of the crack follows the maximum circumferential stress criterion. Erdogan and Sih have provided a calculation formula for the crack deviation angle based on a significant number of experiments [52]:

$$\theta_0(D_{t-n}, D_{t-s}) = \begin{cases} 0 & \text{if } D_{t-s} = 0 \\ 2\arctan\frac{1}{4} \left[\left| \frac{D_{t-n}}{D_{t-s}} \right| - \operatorname{sgn}(D_{t-s}) \sqrt{\left(\frac{D_{t-n}}{D_{t-s}}\right)^2 + 8} \right] & \text{if } D_{t-s} \neq 0, D_{t-n} \neq 0 \\ \arccos\frac{1}{3} & \text{if } D_{t-n} = 0 \end{cases} \quad (6)$$

where D_{t-n}, D_{t-s} is the normal displacement, m, and tangential displacement of tip fracture element, m; θ_0 is the fracture’s deflection angle, °.

2.3. Mode of Multi-Fracture Flow Distribution

When multiple fractures expand at the same time, the fluid flow in each fracture will follow non-uniform distribution. The pressure and flow distribution of each fracture is shown in Figure 1.

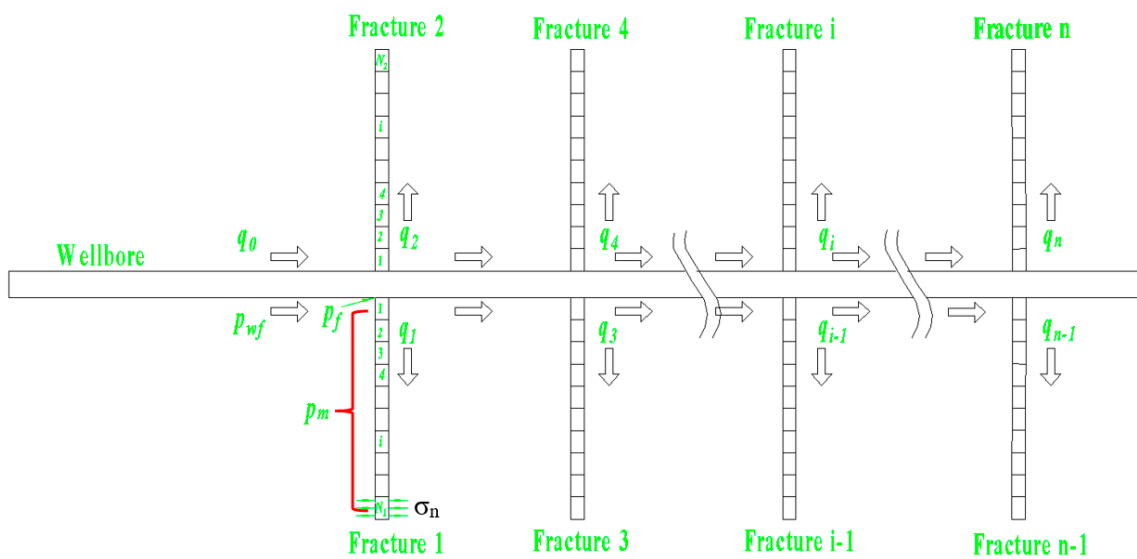


Figure 1. Fluid flow and pressure distribution with multi-crack propagation.

In the process of multi-fracture propagation, part of the injected fluid will flow into the fracture and the other part will filter into the formation. For each fracture, the injection volume, filtration loss and fracture volume satisfy the following mass balance equation:

$$\begin{cases} q_1 \Delta t = \sum_{i=1}^{N_1} \sum_{j=0}^{t+\Delta t} \frac{2hC_L dx_i dt}{\sqrt{t-\tau_i^j}} - \sum_{i=1}^{N_1} \sum_{j=0}^t \frac{2hC_L dx_i dt}{\sqrt{t-\tau_i^j}} + \sum_{i=1}^{N_1} h \Delta w_i \Delta x_i \\ q_2 \Delta t = \sum_{i=1}^{N_2} \sum_{j=0}^{t+\Delta t} \frac{2hC_L dx_i dt}{\sqrt{t-\tau_i^j}} - \sum_{i=1}^{N_2} \sum_{j=0}^t \frac{2hC_L dx_i dt}{\sqrt{t-\tau_i^j}} + \sum_{i=1}^{N_2} h \Delta w_i \Delta x_i \\ \vdots \\ q_n \Delta t = \sum_{i=1}^{N_n} \sum_{j=0}^{t+\Delta t} \frac{2hC_L dx_i dt}{\sqrt{t-\tau_i^j}} - \sum_{i=1}^{N_n} \sum_{j=0}^t \frac{2hC_L dx_i dt}{\sqrt{t-\tau_i^j}} + \sum_{i=1}^{N_n} h \Delta w_i \Delta x_i \end{cases} \quad (7)$$

The total injection rate should be equal to the sum of the flow rate in each fracture, which can be expressed as follows:

$$q_0 = \sum_{i=1}^n q_i \quad (8)$$

where q_0 is the total injection rate, m^3/min ; q_i is the i th fracture injection rate, m^3/min ; w_i is the width of i th fracture element, m; C_L is the fluid loss coefficient, $m/min^{1/2}$; t is injection time, s; h is fracture height, m; τ is the time at which fracture reaches position x .

For multiple fractures expanding simultaneously, the pressure at the entrance of each crack can be calculated as follows [52]:

$$p_{wf} = p_f + p_m + \sigma_n \quad (9)$$

where p_{wf} is the bottom hole pressure, MPa; p_f is the frictional pressure loss in each fracture, MPa; p_m is pressure drop in each fracture, MPa; σ_n is normal stress of the tip fracture, MPa.

The friction of the perforation hole can be calculated as follows:

$$p_f = 2.25 \times 10^{-3} \frac{q_i^2 \rho}{n_p^2 d_f^4 \alpha^2} \quad (10)$$

where q_i is the injection rate of the i th fracture, m^3/min ; ρ is the fluid density, kg/m^3 ; n_p is the number of perforations; d_f is the perforation diameter, m ; α is the discharge coefficient, ranging from 0.8 to 0.89.

Pressure drop in each fracture can be calculated using the Poiseuille equation [36]:

$$p_m = \sum_{j=1}^N 2^{n+1} k \left(\frac{1+2n}{n} \right)^n \left(\frac{q_i}{60 D_n^j h} \right)^n D_n^{j-(n+1)} a_j \quad (11)$$

where q is the injection rate in the fracture, m^3/min ; n is the fluid power-law index; k is the consistency index; μ is the fluid viscosity, $\text{mPa}\cdot\text{s}$; w is the width of the fracture element, m ; h is the fracture height, m .

2.4. Mode of Multi-Fracture-Induced Stress

The induced stress generated by multiple crack expansion can be calculated as the following expression [57]:

$$\begin{cases} \sigma_{xx} = \sum_{j=1}^N F^{ij} A_{xx}^{ij} D_v^j + \sum_{j=1}^N F^{ij} A_{xy}^{ij} w_n^j \\ \sigma_{yy} = \sum_{j=1}^N F^{ij} A_{yx}^{ij} D_v^j + \sum_{j=1}^N F^{ij} A_{yy}^{ij} w_n^j \\ \tau_{xy} = \sum_{j=1}^N F^{ij} A_{sx}^{ij} D_v^j + \sum_{j=1}^N F^{ij} A_{sy}^{ij} w_n^j \end{cases} \quad (12)$$

where σ_{xx} is the induced stress in the x direction, MPa; σ_{yy} is the induced stress in the y direction, MPa; τ_{xy} is the induced shear stress, MPa; A_{xx}^{ij} , A_{xy}^{ij} , A_{yx}^{ij} , A_{yy}^{ij} , A_{sx}^{ij} , A_{sy}^{ij} are the boundary-influence coefficients matrix for the stresses of fracture element; F_{ij} is a fracture stress correction factor; Subscript i, j is the fracture element number; D_n is the normal displacement of fracture element, m ; D_s is the tangential displacement of fracture element, m .

3. Model Solution and Verification

3.1. Model Solution

The above model involves rock deformation, competitive extension and redirection of multiple fractures, as well as dynamic distribution of fluid flow. The coupling between fluid pressure and stress field is also considered, and an iterative method is commonly used to calculate normal and tangential displacements of fracture elements, fluid pressure within the fractures, displacement of each fracture and induced stress distribution. Firstly, the parameters of hydraulic fractures can be solved by the displacement discontinuity method (DDM). Then, based on the known parameters, the flow rate, pressure and induced stress distribution of each fracture are calculated. The detail solution process involves the following steps:

(1) Determine the initial coordinates of fracture elements based on the initial perforation center position.

(2) Assume an initial injection pressure and use the fracture deformation equation and the DDM to calculate the normal displacement (fracture width) and tangential displacement of each fracture element.

(3) Based on the width and length of each fracture element, as well as the total injection time and injection rate, the flow rate of each fracture can be calculated according to the mass balance equation.

(4) The friction of the perforation hole, the pressure drop within the fracture, the pressure at the fracture tip element and the injection pressure can be calculated with Equations (9)–(11).

(5) The calculated injection pressure and the guessing initial injection pressure are compared to verify the convergence. If the convergence criterion is not satisfied, the guessing value is modified as $p_0 = \omega p_i + (1 - \omega) p_0$, and then the (1)–(5) process is repeated until the convergence is satisfied.

(6) Calculate induced stress based on the fracture parameters and fracture element coordinates.

(7) Repeat steps 2–6 until the desired fracture length is achieved.

According to the above process, the iteratively coupled solution is compiled by using the MATLAB development platform. The program design flow is illustrated in Figure 2.

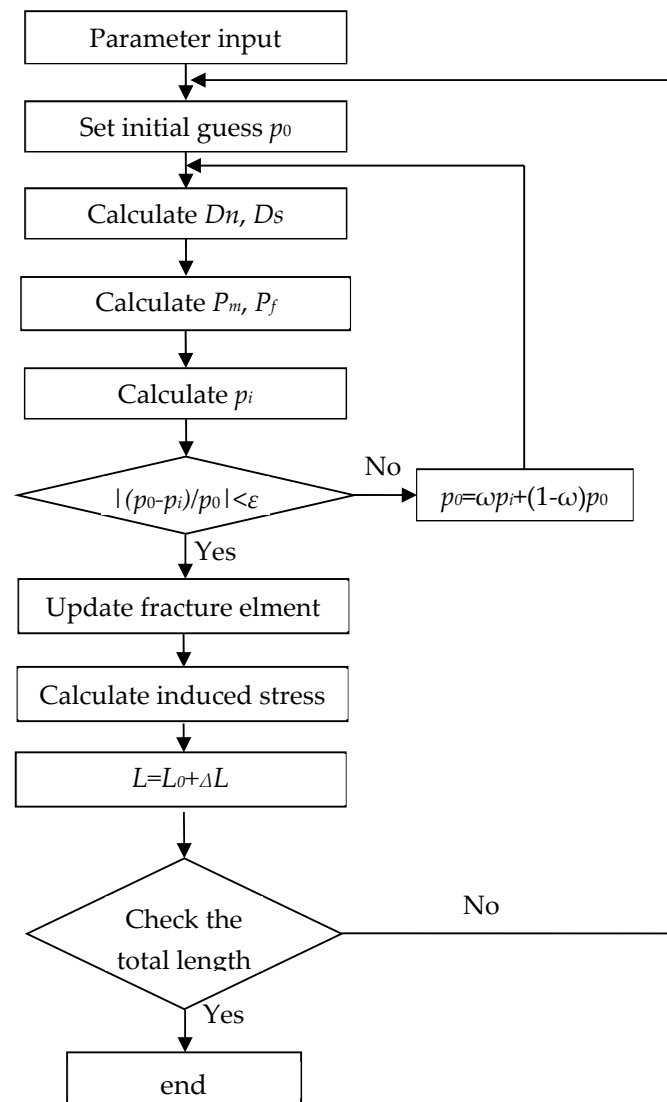


Figure 2. The solving flowchart of the multi-fracture propagation model.

3.2. Model Verification

Sneddon revealed analytical solutions for the width distribution of individual cracks and the induced stress at any position along the symmetry axis of the crack [58]. To validate the model, we compared the calculated results of crack width and induced stress between our model and Sneddon's analytical model. It is assumed that the injected pressure is 3 MPa, the crack length is 80 m, the rock's Poisson's ratio is 0.25 and Young's modulus is 25,000 MPa. The fracture element number is set to 40, 20 and 10. The comparative results for different numbers of elements are shown in Figure 3.

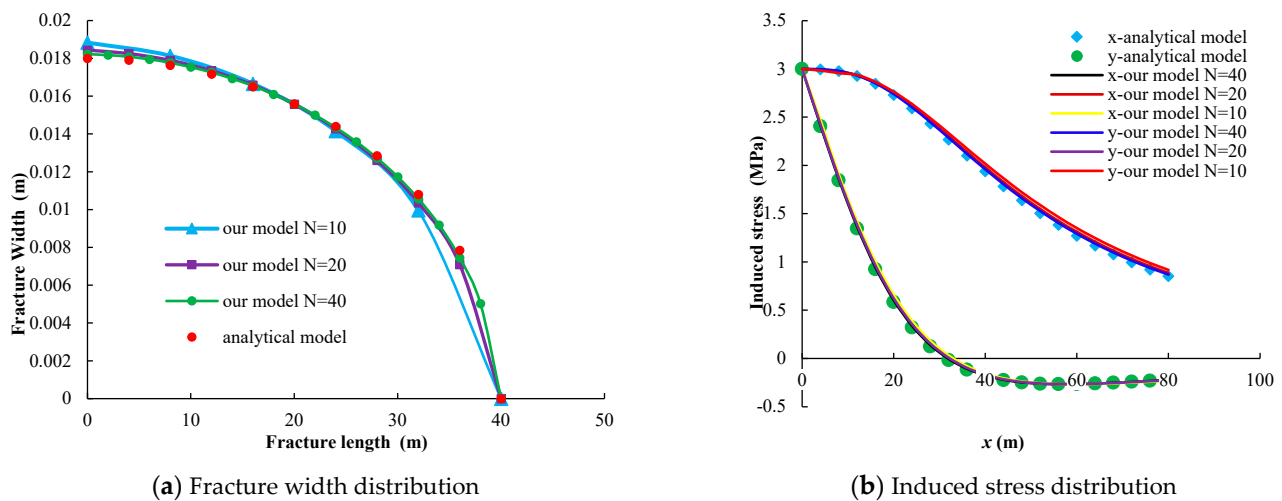


Figure 3. Comparison of fracture width and induced stress distribution for two models.

Figure 3 indicates that the calculated results of this model are basically consistent with Sneddon's analytical model, and the width distribution in the crack and the induced stress in the x and y directions on the symmetry axis are roughly the same. The number of discrete elements has little influence on the calculated results of the model, and the calculated result is effective and reliable.

4. Numerical Results and Discussion

4.1. Effect of Perforation Cluster Number on Multi-Fracture Propagation

Perforation cluster number is a critical factor for multi-fracture propagation. It has a significant influence on fracture morphology, flow distribution, bottom hole pressure and induced stress distribution. To reveal the specific mechanism, it is assumed that the number of perforation clusters is three, four, and five, respectively, the injection rate is $12 \text{ m}^3/\text{min}$, the fracture toughness of rock is $1.5 \text{ MPa}\cdot\text{m}^{0.5}$, the fracture height is 20 m, the fracturing fluid viscosity is $2 \text{ mPa}\cdot\text{s}$, the filtration coefficient is $0.00054 \text{ m}/\text{min}^{0.5}$, the number of perforations of each cluster is six, the perforation hole diameter is 10 mm and the cluster spacing is 10 m. The calculation results are presented in Figures 4–6.

Figure 4 indicates that, under the same perforation cluster number, all the cracks follow non-uniform propagation, resulting short and narrow inner cracks and wide and long exterior cracks. The higher the number of perforating clusters, the more serious the interior fracture will be. As the number of perforating clusters increased to four, the inner fracture almost stopped expanding. For a three-cluster perforation, the increase in the middle fracture length will also have great effect on the injection point of the outer fracture, resulting in a narrow injection point of the outer fracture. Figure 5 shows that, as the number of perforating clusters increases, the inner fracture will receive much less fluid, which will further limit the growth of the inner cracks. Due to the fact that the induced stress adds additional compressional stress on the inner fractures, the exterior fractures tend to receive more fluid while the interior fracture receives less, exhibiting a short and narrow fracture. Figure 6 illustrates that the bottom hole pressure increases with the increase in the

number of perforating clusters, because the increasing perforating clusters number will lead to a decrease in perforating friction.

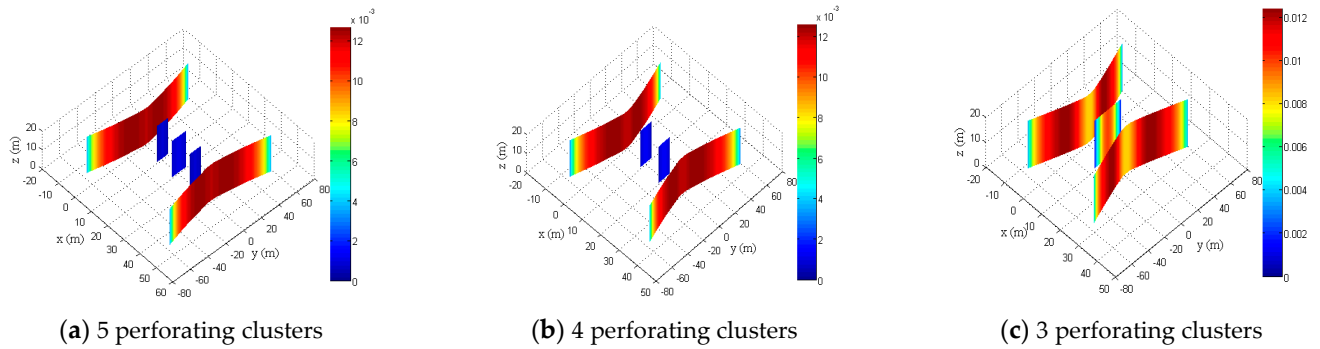


Figure 4. Effect of perforation cluster number on fracture shape.

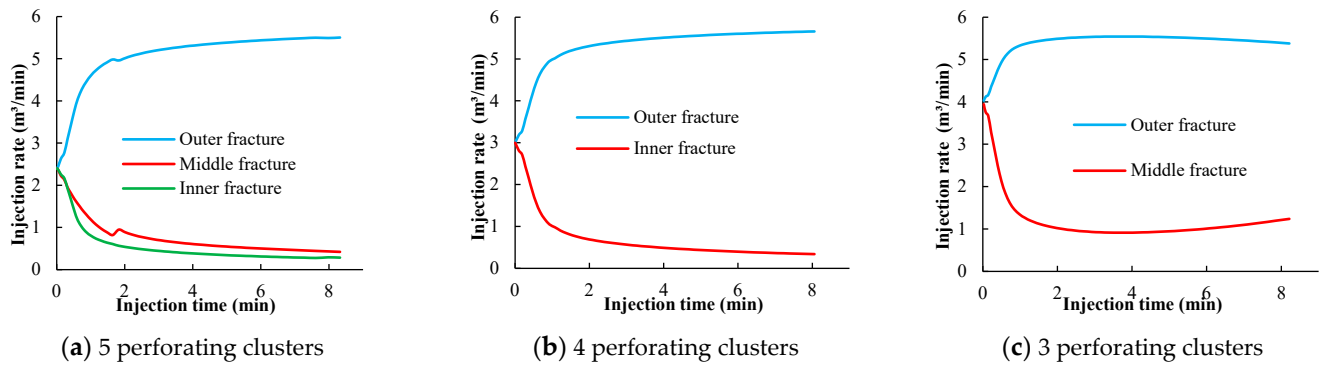


Figure 5. Effect of perforation cluster number on the flow of fracture.

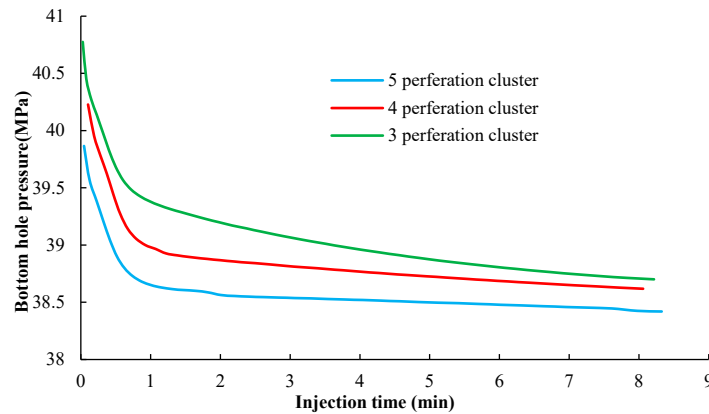


Figure 6. Effect of perforation cluster number on the bottom hole pressure.

Figure 7 presents that the induced stress generated by the inner crack in the x direction increases with the increasing number of perforating clusters, and the inner cracks are squeezed more severely, resulting in a more difficult crack propagating and less flow distribution. The decrease in the number of perforation clusters also leads to the decrease in induced stress in y direction and shear stress in inner crack tip, as well as the decrease in the lateral crack deflection angle. This is because, when the inner crack growth is inhibited, the induced stress will also be reduced.

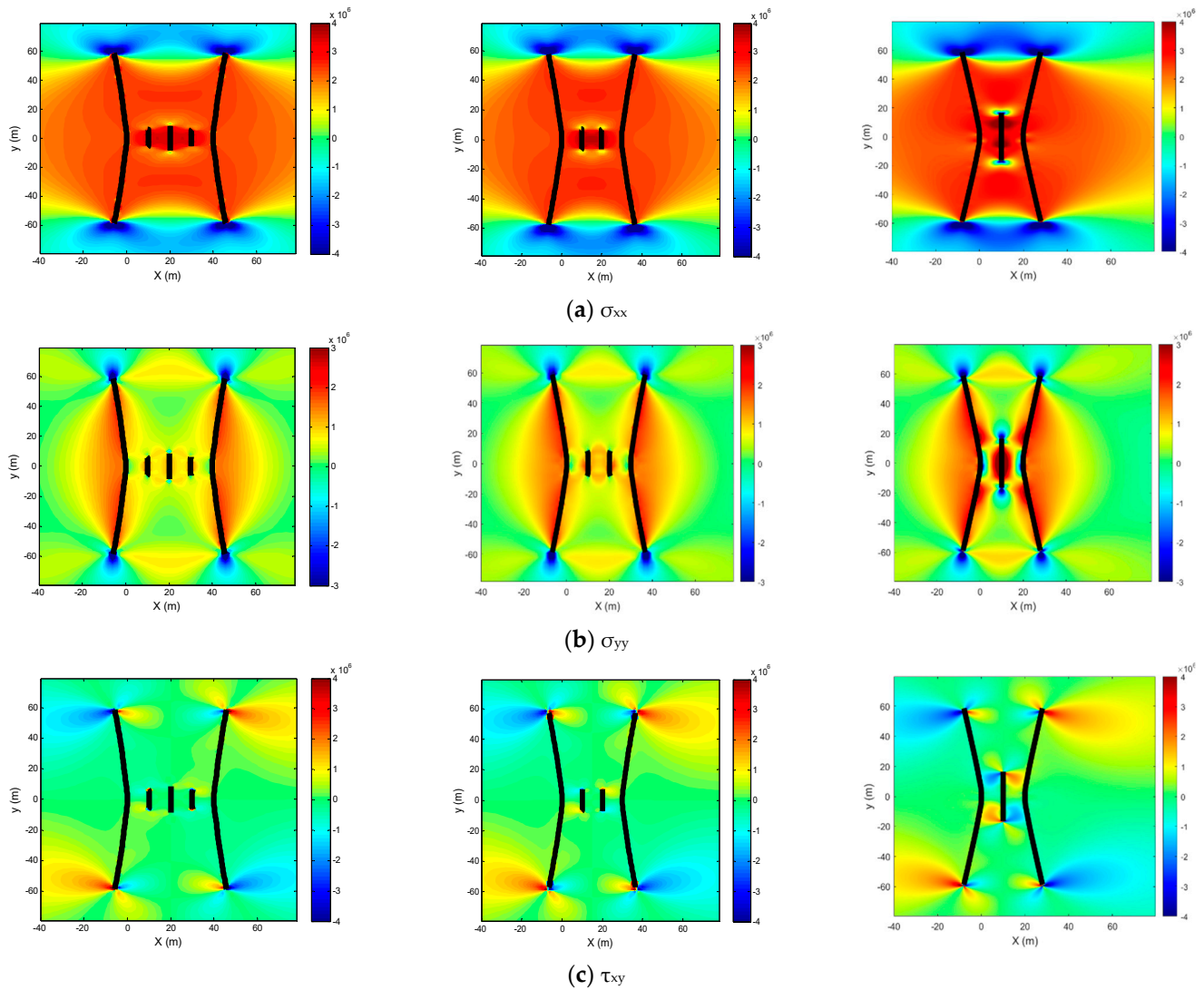


Figure 7. Effect of perforation cluster number on the induced stress.

4.2. Effect of Cluster Spacing on Multi-Fracture Propagation

Perforation cluster spacing also has influence on fracture propagation. To reveal the specific mechanism, the effects of cluster spacing on multi-fracture morphology, flow distribution, bottom hole pressure and induced stress distribution are studied based on five cluster perforations. It is assumed that the perforation diameter is 10 mm, the cluster spacing is 10 m, 15 m and 20 m, respectively, and other parameters are the same as in Section 4.1. The simulation results are presented in Figures 8–13.

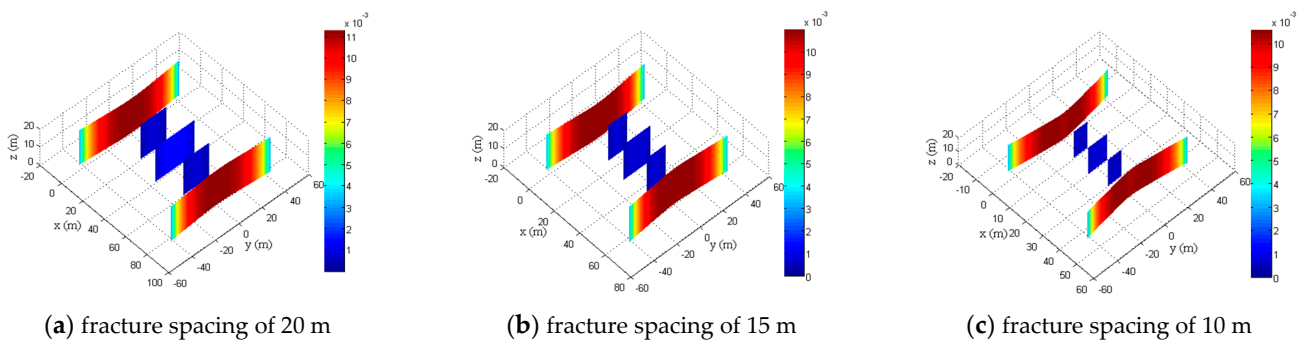


Figure 8. Effect of perforation cluster distance on fracture shape.

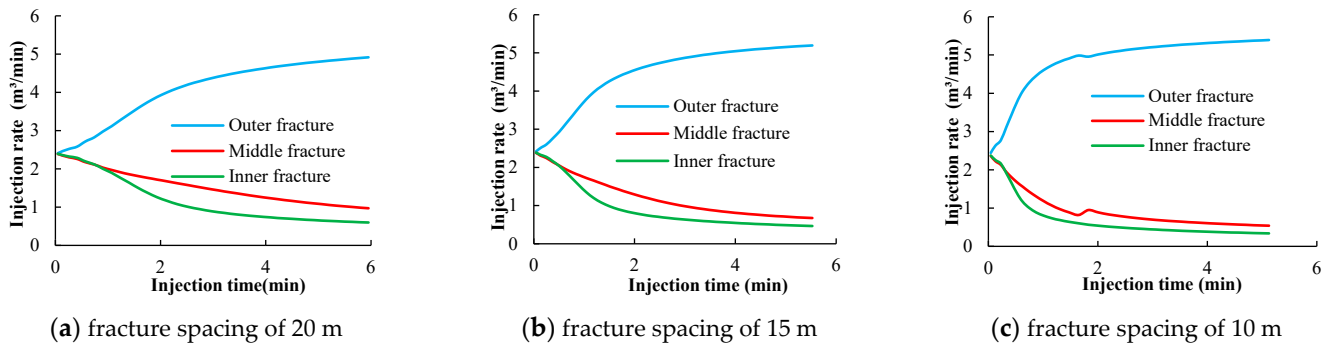


Figure 9. Effect of perforation cluster distance on the flow of fracture.

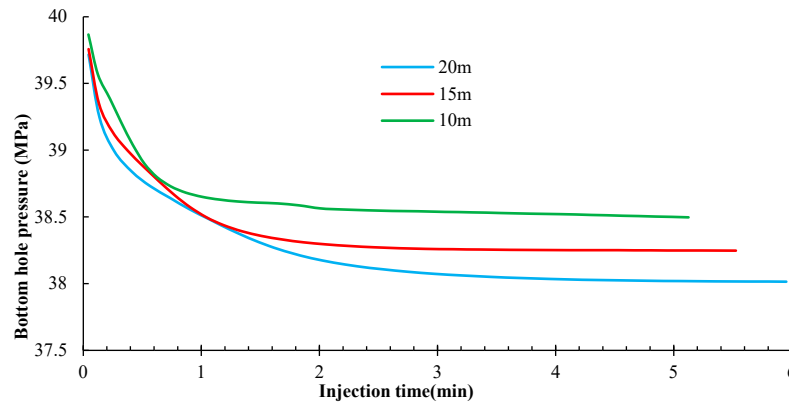


Figure 10. Effect of perforation cluster distance on the bottom hole pressure.

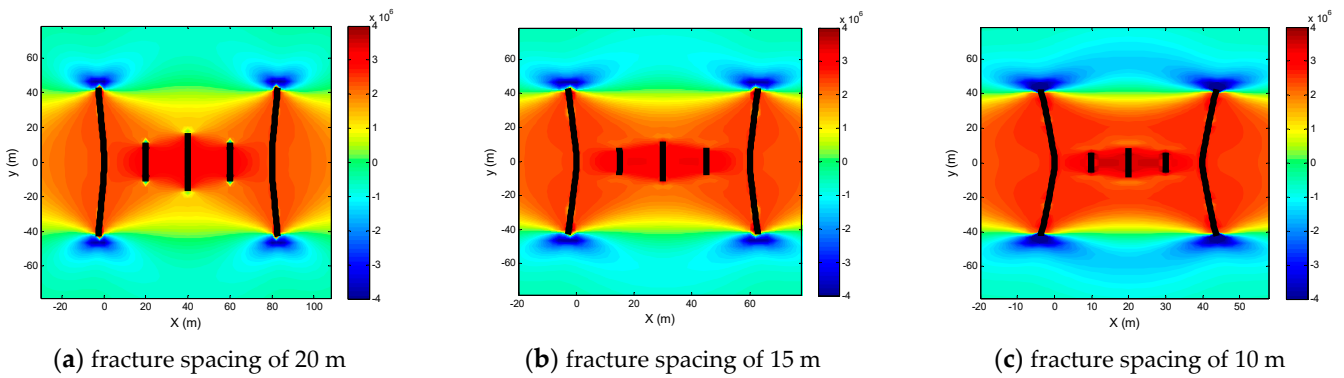


Figure 11. Effect of perforation cluster distance on the induced stress σ_{xx} .

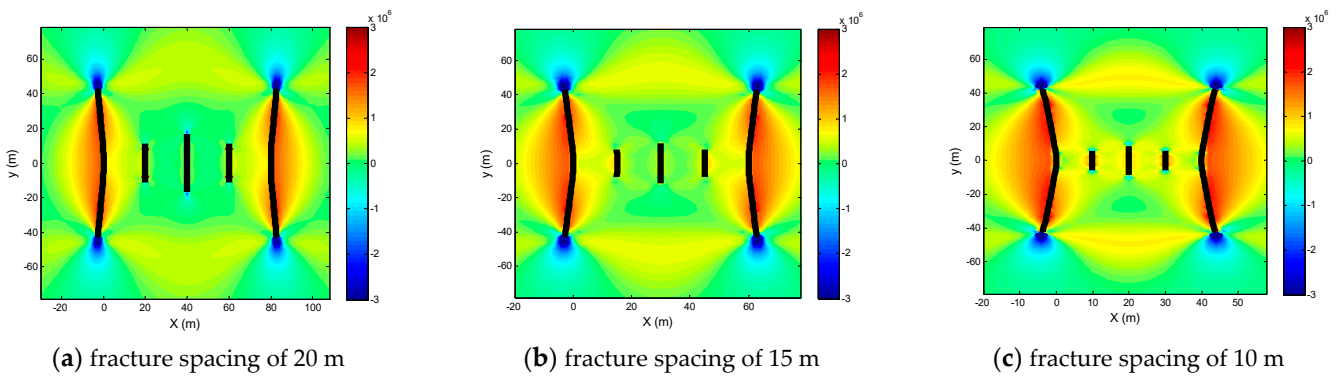


Figure 12. Effect of perforation cluster distance on the induced stress σ_{yy} .

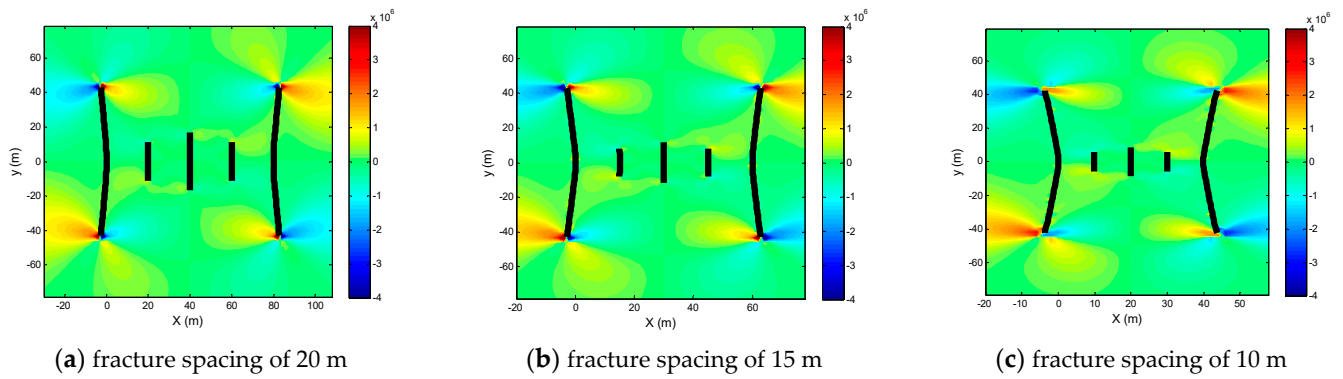


Figure 13. Effect of perforation cluster distance on the induced stress τ_{xy} .

Figure 8 illustrates that, for different cluster spacing, the expansion velocity of the inner and middle fractures is lower than that of the outer cracks. Moreover, as the perforation spacing increases, the inner and middle cracks exhibit wider and longer characteristics.

Figure 9 indicates that, with the increase in perforation cluster spacing, the flow distribution in the inner and middle fractures increases, but the flow from the outer fractures still dominates, and the flow from the inner and middle fractures decreases with the expansion of the fractures. Figure 10 displays that the bottom hole pressure decreases with the increase in the spacing of perforating clusters. This is because the stress interference between fractures decreases with the increase in the spacing of clusters, resulting in the increase in fracture width and the decrease in fracture friction.

As shown in Figures 11–13, with the increase in cluster spacing, the induced stress and shear stress generated by the inner and middle fracture in the x and y directions gradually decrease, as does the stress interference and the outward migration angle of the outer crack. The decrease in stress interference between fractures leads to the increase in the width and flow rate of inner and middle fractures, and the decrease in bottom hole pressure. Therefore, increasing cluster spacing is beneficial to reduce stress interference between the inner fractures, promote flow distribution of the interior fractures and reduce fracture pressure.

4.3. Effect of Perforation Diameter on Multi-Fracture Propagation

Perforation diameter also plays important roles in fracture design. The effect of perforation diameter on fracture morphology, flow distribution, bottom hole pressure and induced stress distribution is investigated based on four perforation clusters. It is assumed that cluster spacing is 15 m, perforation diameters are 7 mm, 8 mm and 10 mm, respectively, and other parameters are the same as in Section 4.1. The calculation results are shown in Figures 14–19.

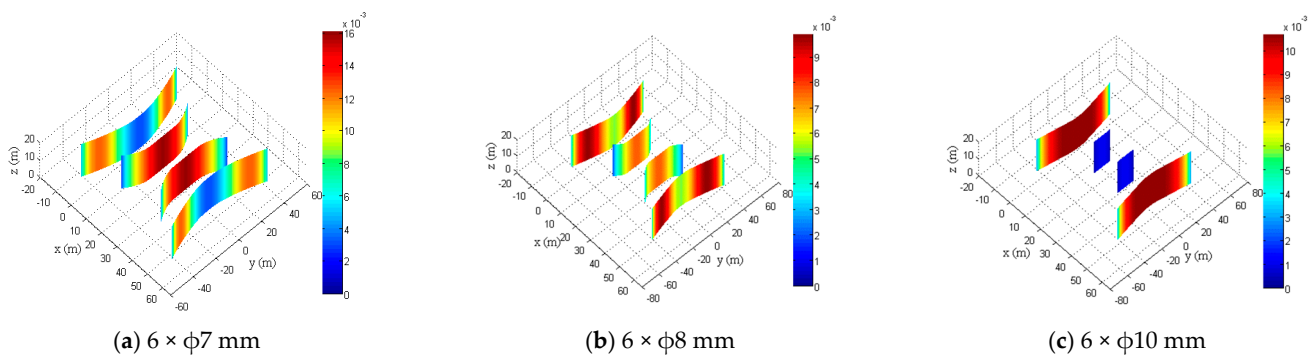


Figure 14. Effect of perforation diameter on fracture shape.

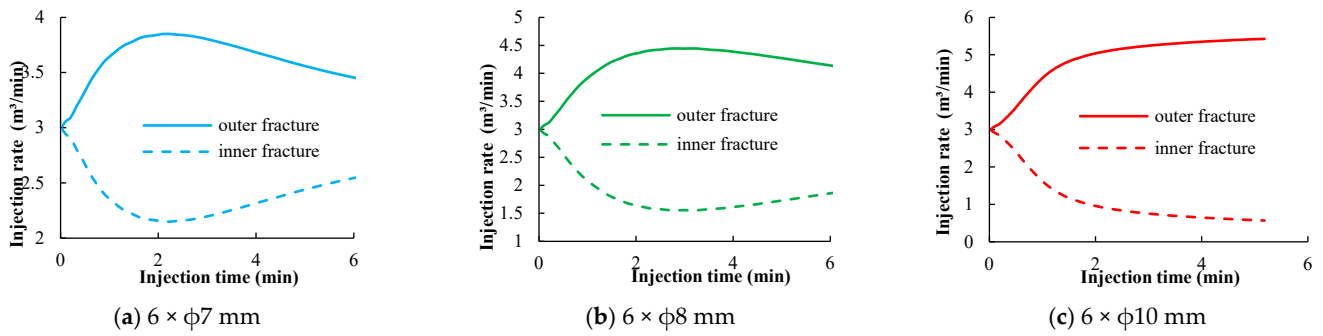


Figure 15. Effect of perforation diameter on the flow of fracture.

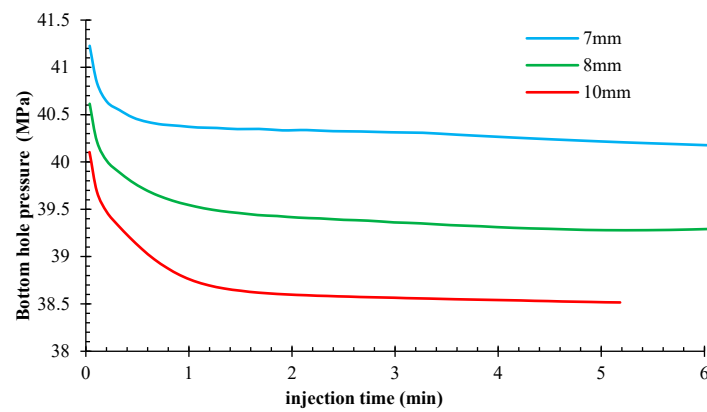


Figure 16. Effect of perforation diameter on the bottom hole pressure.

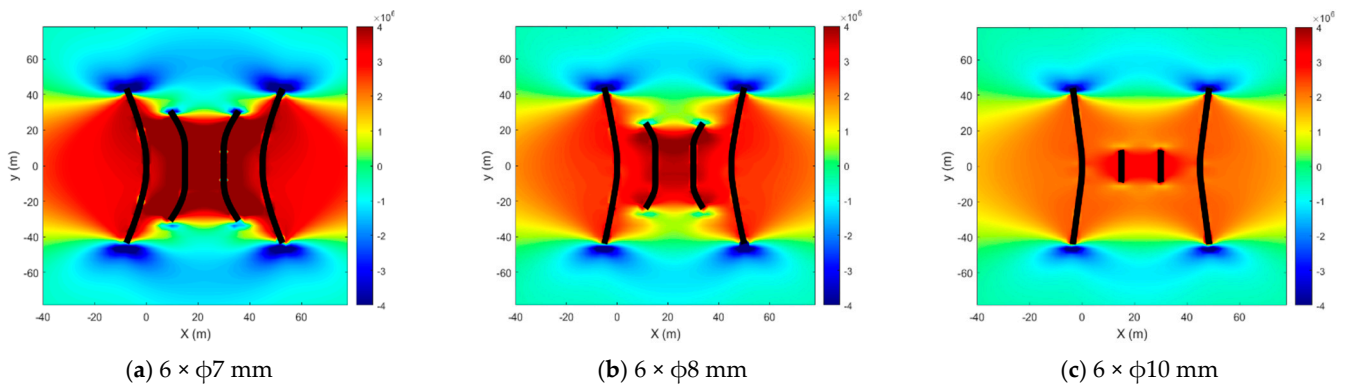


Figure 17. Effect of perforation diameter on the induced stress σ_{xx} .

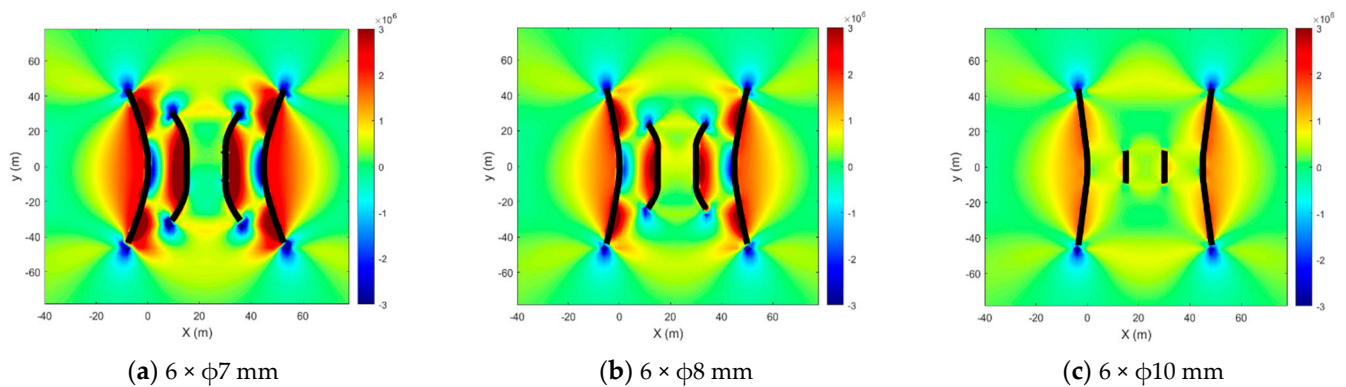


Figure 18. Effect of perforation diameter on the induced stress σ_{yy} .

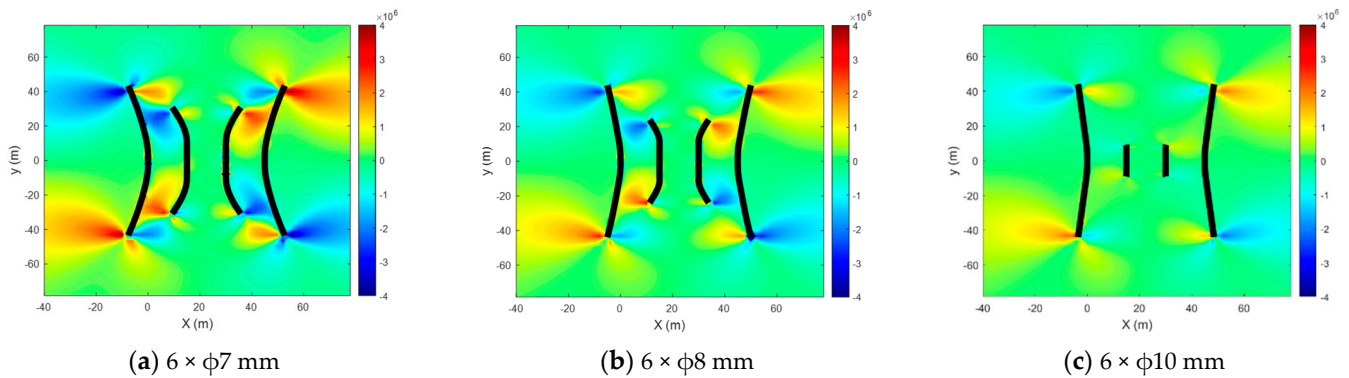


Figure 19. Effect of perforation diameter on the induced stress τ_{xy} .

Figure 14 presents that, for four cracks extending simultaneously, non-uniform growth still occurs. With the decrease in the perforation diameter, the length and width of the inner fracture increase gradually, while the width of the outer fracture gradually decreases, and the induced stress caused by the inner fracture has an increased interference effect on the outer fracture. Figures 15 and 16 illustrate that, with the decrease in perforation diameter, the perforation friction increases, resulting in a gradual increase in the flow distributed of the inner crack and decrease in the bottom hole pressure.

Figures 17–19 indicate that, with the increase in perforation diameter, the induced stress and induced shear stress of the outer fractures in the x and y directions gradually decrease, while that of the inner fractures increase, resulting in a gradual increase in the width of the outer crack and the migration angle of the inner crack, as well as short and narrow inner cracks. Therefore, reducing the perforation diameter is conducive to the expansion and flow distribution of the inner crack, but it will increase the construction pressure.

5. Conclusions

(1) Based on the interaction of rock deformation, multi-fracture competitive propagation and steering, multi-fracture flow and multi-fracture stress interference, a fluid–structure coupling multi-fracture propagation model and solution program are established. The calculation results of the model are consistent with the analytical model, and the algorithm is stable and reliable.

(2) As the number of perforating clusters increases, the inner fracture propagation is inhibited more severely, resulting in short and narrow fracture geometry, and little flow distribution, as well as low bottom hole pressure. The induced stress of the inner crack is greater than that of the outer crack in the x direction, while the induced stress and shear stress in the y direction are lower than that of the outer fracture. Owing to the induced stress interference, the flow distribution in the inner fracture is less than that in the outer fracture.

(3) With the increase in cluster spacing, the induced stress among fractures and the deflection angle of the outer fractures decreases gradually, while the flow distribution of the inner fractures increases, resulting in less bottom hole pressure. Increasing the cluster spacing is conducive to reducing the stress interference, promoting the flow distribution of the inner fracture and reducing the fracture pressure.

(4) With the decrease in the perforation diameter, the inner fracture expansion velocity and flow distribution and bottom hole pressure increase, while the inlet width and flow of the outer fracture decrease. A small perforation diameter is beneficial to uniform flow distribution and fracture geometry, but will lead to great perforating friction and fracturing pressure, as well as inner fracture turning.

Author Contributions: Conceptualization, J.Z. and X.Z.; methodology, H.W. and X.Z.; validation, J.Z. and X.Z.; formal analysis, H.W. and X.Z.; investigation, J.Z.; resources, X.Z. and Y.L.; data curation, J.Z.; writing—original draft preparation, J.Z.; writing—review and editing, X.Z. and J.Z.; visualization, J.Z. and Y.L.; supervision, H.W. and X.Z.; project administration, J.Z. and X.Z.; funding acquisition, J.Z. All authors have read and agreed to the published version of the manuscript.

Funding: This work was supported by the financial support of the National Natural Science Foundation of China (52204025), Open Fund (PLN2022-18) State Key Laboratory of Oil and Gas Reservoir Geology and Exploitation, Southwest Petroleum University and China and Chengdu North Petroleum Exploration and Development Technology Co., Ltd. cooperation project: Research on fracturing optimization based on machine learning method (ZH001).

Data Availability Statement: The data presented in this study are available from the corresponding author on reasonable request.

Acknowledgments: The authors extend their gratitude for the financial support received from the China Government.

Conflicts of Interest: Author Xing Zhao and Hehua Wang were employed by the company China & Chengdu North Petroleum Exploration and Development Technology. Author Yuandong Liu was employed by the company China Petroleum Technology and Development Company. Author Xing Zhao was employed by the company China Zhenhua Oil Company Limited. The remaining authors declare that the research was conducted in the absence of any commercial or financial relationships that could be construed as a potential conflict of interest.

References

- Niu, W.; Lu, J.; Sun, Y.; Liu, H.; Cao, X.; Zhan, H.; Zhang, J. A review of the application of data-driven technology in shale gas production evaluation. *Energy Rep.* **2023**, *10*, 213–227. [[CrossRef](#)]
- Li, H. Coordinated development of shale gas benefit exploitation and ecological environmental conservation in China: A mini review. *Front. Ecol. Evol.* **2023**, *11*, 1232395. [[CrossRef](#)]
- Liu, J.; Bai, X.; Elsworth, D. Evolution of pore systems in low-maturity oil shales during thermal upgrading—Quantified by dynamic SEM and machine learning. *Pet. Sci.* **2023**, 12283, *in press*. [[CrossRef](#)]
- Montgomery, C.T.; Smith, M.B. Hydraulic fracturing: History of an enduring technology. *J. Pet. Technol.* **2010**, *62*, 26–40. [[CrossRef](#)]
- Lecampion, B.; Desroches, J. Simultaneous initiation and growth of multiple radial hydraulic fractures from a horizontal wellbore. *J. Mech. Phys. Solids* **2015**, *82*, 235–258. [[CrossRef](#)]
- Xu, Y.; Lun, Z.; Pan, Z.; Wang, H.; Zhou, X.; Zhao, C.; Zhang, D. Occurrence space and state of shale oil: A review. *J. Pet. Sci. Eng.* **2022**, *211*, 110183. [[CrossRef](#)]
- Zia, H.; Lecampion, B. Explicit versus implicit front advancing schemes for the simulation of hydraulic fracture growth. *Int. J. Numer. Anal. Methods Geomech.* **2019**, *43*, 1300–1315. [[CrossRef](#)]
- Tang, H.; Wang, S.; Zhang, R.; Li, S.; Zhang, L.; Wu, Y.-S. Analysis of stress interference among multiple hydraulic fractures using a fully three-dimensional displacement discontinuity method. *J. Pet. Sci. Eng.* **2019**, *179*, 378–393. [[CrossRef](#)]
- Cherny, S.; Lapin, V.; Esipov, D.; Kuranakov, D.; Avdyushenko, A.; Lyutov, A.; Karnakov, P. Simulating fully 3D non-planar evolution of hydraulic fractures. *Int. J. Fract.* **2016**, *66*, 181–211. [[CrossRef](#)]
- Lu, G.; Gordeliy, E.; Prioul, R.; Aidagulov, G.; Bungler, A. Modeling simultaneous initiation and propagation of multiple hydraulic fractures under subcritical conditions. *Comput. Geotech.* **2018**, *104*, 196–206. [[CrossRef](#)]
- Dontsov, E.V.; Suarez-Rivera, R. Propagation of multiple hydraulic fractures in different regimes. *Int. J. Rock Mech. Min. Sci.* **2020**, *128*, 104270. [[CrossRef](#)]
- Fan, H.; Li, S.; Feng, X.-T.; Zhu, X. A high-efficiency 3D boundary element method for estimating the stress/displacement field induced by complex fracture networks. *J. Pet. Sci. Eng.* **2020**, *187*, 106815. [[CrossRef](#)]
- Gordeliy, E.; Peirce, A.P. Enrichment strategies and convergence properties of the XFEM for hydraulic fracture problems. *Comput. Methods Appl. Mech. Eng.* **2015**, *283*, 474–502. [[CrossRef](#)]
- Gordeliy, E.; Detournay, E. A fixed grid algorithm for simulating the propagation of a shallow hydraulic fracture with a fluid lag. *Int. J. Numer. Methods Eng.* **2010**, *35*, 602–629. [[CrossRef](#)]
- Mohammadnejad, T.; Khoei, A.R. An extended finite element method for hydraulic fracture propagation in deformable porous media with the cohesive crack model. *Finite Elem. Anal. Des.* **2013**, *73*, 77–95. [[CrossRef](#)]
- Duan, K.; Kwok, C.Y.; Zhang, Q.; Shang, J. On the initiation, propagation and reorientation of simultaneously-induced multiple hydraulic fractures. *Comput. Geotech.* **2020**, *117*, 103226. [[CrossRef](#)]
- Yan, C.; Gao, Y.; Guo, H. A FDEM based 3D discrete mixed seepage model for simulating fluid driven fracturing. *Eng. Anal. Bound. Elem.* **2022**, *140*, 447–463. [[CrossRef](#)]
- Cundall, P.A.; Strack, O. A discrete numerical model for granular assemblies. *Geotechnique* **1979**, *29*, 47–65. [[CrossRef](#)]

19. Belytschko, T.; Black, T. Elastic crack growth in finite elements with minimal remeshing. *Int. J. Numer. Methods Eng.* **1999**, *45*, 601–620. [[CrossRef](#)]
20. Belytschko, T.; Lu, Y.Y.; Gu, L. Element-free galerkin methods. *Int. J. Numer. Methods Eng.* **1994**, *37*, 229–256. [[CrossRef](#)]
21. Belytschko, T.; Gracie, R.; Ventura, G. A review of extended/generalized finite element methods for material modeling. *Model. Simul. Mater. Sci. Eng.* **2009**, *17*, 043001. [[CrossRef](#)]
22. Benz, W.; Asphaug, E. Simulations of brittle solids using smooth particle hydrodynamics. *Comput. Phys. Commun.* **1995**, *87*, 253–265. [[CrossRef](#)]
23. Giner, E.; Sukumar, N.; Tarancón, J.E.; Fuenmayor, F.J. An Abaqus implementation of the extended finite element method. *Eng. Fract. Mech.* **2009**, *76*, 347–368. [[CrossRef](#)]
24. Gupta, P.; Duarte, C.A. Simulation of non-planar three-dimensional hydraulic fracture propagation. *Int. J. Numer. Anal. Methods Geomech.* **2014**, *38*, 1397–1430. [[CrossRef](#)]
25. Gupta, P.; Duarte, C.A. Coupled formulation and algorithms for the simulation of non-planar three-dimensional hydraulic fractures using the generalized finite element method. *Int. J. Numer. Anal. Methods Geomech.* **2016**, *40*, 1402–1437. [[CrossRef](#)]
26. Khoei, A.R.; Hirmand, M.; Vahab, M.; Bazargan, M. An enriched FEM technique for modeling hydraulically driven cohesive fracture propagation in impermeable media with frictional natural faults: Numerical and experimental investigations. *Int. J. Numer. Methods Eng.* **2015**, *104*, 439–468. [[CrossRef](#)]
27. Wang, H. Numerical Modeling of Non-Planar Hydraulic Fracture Propagation in Brittle and Ductile Rocks using XFEM with Cohesive Zone Method. *J. Pet. Sci. Eng.* **2016**, *135*, 127–140. [[CrossRef](#)]
28. Faivre, M.; Paul, B.; Golfier, F.; Giot, R.; Massin, P.; Colombo, D. 2D coupled HMXFEM modeling with cohesive zone model and applications to fluid-driven fracture network. *Eng. Fract. Mech.* **2016**, *159*, 115–143. [[CrossRef](#)]
29. Salimzadeh, S.; Usui, T.; Paluszny, A.; Zimmerman, R.W. Finite element simulations of interactions between multiple hydraulic fractures in a poroelastic rock. *Int. J. Rock Mech. Min. Sci.* **2017**, *99*, 9–20. [[CrossRef](#)]
30. Weng, X.; Kresse, O.; Chuprakov, D.; Cohen, C.-E.; Prioul, R.; Ganguly, U. Applying complex fracture model and integrated workflow in unconventional reservoirs. *J. Pet. Sci. Eng.* **2014**, *124*, 468–483. [[CrossRef](#)]
31. Hui, G.; Chen, Z.; Schultz, R.; Chen, S.; Song, Z.; Zhang, Z.; Song, Y.; Wang, H.; Wang, M.; Gu, F. Intricate unconventional fracture networks provide fluid diffusion pathways to reactivate pre-existing faults in unconventional reservoirs. *Energy* **2023**, *282*, 128803. [[CrossRef](#)]
32. Deng, S.; Li, H.; Ma, G.; Huang, H.; Li, X. Simulation of shale–proppant interaction in hydraulic fracturing by the discrete element method. *Int. J. Rock Mech. Rock Eng.* **2014**, *70*, 219–228. [[CrossRef](#)]
33. Huang, H.; Detournay, E. Intrinsic length scales in tool-rock interaction. *Int. J. Geomech.* **2008**, *8*, 39–44. [[CrossRef](#)]
34. Zou, Y. Numerical investigation of hydraulic fracture network propagation in naturally fractured shale formations. *J. Struct. Geol.* **2016**, *84*, 1–13. [[CrossRef](#)]
35. Wu, K.; Olson, J.E. Simultaneous Multifracture Treatments: Fully Coupled Fluid Flow and Fracture Mechanics for Horizontal Wells. *SPE J.* **2015**, *20*, 337–346. [[CrossRef](#)]
36. Wu, K. Numerical Modeling of Complex Hydraulic Fracture Development in Unconventional Reservoirs. Ph.D. Thesis, University of Texas at Austin, Austin, TX, USA, 2014.
37. Zhang, X.; Wu, B.; Jeffrey, R.G.; Connell, L.D.; Zhang, G. A new pseudo-3D model for hydraulic fracture growth in a multilayered rock. *International Journal of Solids and Structures*. *Int. J. Solids Struct.* **2017**, *116*, 208–223.
38. Zhang, X.; Wu, B.; Connell, L.D.; Han, Y.; Jeffrey, R.G. A model for hydraulic fracture growth across multiple elastic layers. *J. Pet. Sci. Eng.* **2018**, *167*, 918–928. [[CrossRef](#)]
39. Kresse, O.; Weng, X. Numerical modeling of 3D hydraulic fractures interactions in complex naturally fractured formations. *Rock Mech. Rock Eng.* **2018**, *51*, 3863–3881. [[CrossRef](#)]
40. Peirce, A.P.; Dontsov, E. An implicit level set method for modeling hydraulically driven fractures. *Comput. Methods Appl. Mech. Eng.* **2008**, *197*, 2858–2885. [[CrossRef](#)]
41. Dontsov, E.; Peirce, A.P. An enhanced pseudo-3D model for hydraulic fracturing accounting for viscous height growth, non-local elasticity, and lateral toughness. *Eng. Fract. Mech.* **2015**, *142*, 116–139. [[CrossRef](#)]
42. Mohammadnejad, T.; Andrade, J.E. Numerical modeling of hydraulic fracture propagation, closure and reopening using XFEM with application to in-situ stress estimation. *Int. J. Numer. Anal. Methods Geomech.* **2016**, *40*, 2033–2060. [[CrossRef](#)]
43. Shimizu, H.; Murata, S.; Ishida, T. The distinct element analysis for hydraulic fracturing in hard rock considering fluid viscosity and particle size distribution. *Int. J. Rock Mech. Min. Sci.* **2011**, *48*, 712–727. [[CrossRef](#)]
44. Shimizu, H.; Ito, T.; Tamagawa, T.; Tezuka, K. A study of the effect of brittleness on hydraulic fracture complexity using a flow-coupled discrete element method. *J. Pet. Sci. Eng.* **2018**, *160*, 372–383. [[CrossRef](#)]
45. Zhang, F.; Dontsov, E.V.; Mack, M. Fully coupled simulation of a hydraulic fracture interacting with natural fractures with a hybrid discrete-continuum method. *Int. J. Numer. Anal. Methods Geomech.* **2017**, *41*, 1430–1452. [[CrossRef](#)]
46. Zhang, F.; Zhu, H.; Zhou, H.; Guo, J.; Huang, B. Discrete-element-method computational-fluid-dynamics coupling simulation of proppant embedment and fracture conductivity after hydraulic fracturing. *SPE J.* **2017**, *22*, 632–644. [[CrossRef](#)]
47. Zhang, F.; Dontsov, E. Modeling hydraulic fracture propagation and proppant transport in a two-layer formation with stress drop. *Eng. Fract. Mech.* **2018**, *199*, 705–720. [[CrossRef](#)]

48. Zhang, F.; Mack, M. Integrating fully coupled geomechanical modeling with microseismicity for the analysis of refracturing treatment. *J. Nat. Gas Sci. Eng.* **2017**, *46*, 16–25. [[CrossRef](#)]
49. Zhang, F.; Damjanac, B.; Maxwell, S. Investigating hydraulic fracturing complexity in naturally fractured rock masses using fully coupled multiscale numerical modeling. *Rock Mech. Rock Eng.* **2019**, *52*, 5137–5160. [[CrossRef](#)]
50. Hu, Y.; Zhao, J.; Cao, L.; Zhao, J.; Li, J.; Wu, Z.; Hou, J. Numerical Simulation for fracture propagation in elastoplastic formations. *Geofluids* **2021**, *2021*, 6680023. [[CrossRef](#)]
51. Chen, X.; Zhao, J.; Yan, W.; Zhang, X. Numerical investigation into the simultaneous growth of two closely spaced fluid-driven fractures. *SPE J.* **2019**, *24*, 274–289. [[CrossRef](#)]
52. Zhao, J.; Zhao, J.; Hu, Y.; Huang, T.; Zhao, X.; Liu, X. Non-planar fracture propagation model for fluid-driven fracturing based on fluid-solid coupling. *Eng. Fract. Mech.* **2020**, *235*, 107159. [[CrossRef](#)]
53. Zhao, J.; Zhao, X.; Zhao, J.; Cao, L.; Hu, Y.; Liu, X. Coupled model for simulating proppant distribution in extending fracture. *Eng. Fract. Mech.* **2021**, *253*, 107865. [[CrossRef](#)]
54. Zhang, S.; Lei, X.; Zou, Y.; Xu, G. Numerical simulation of hydraulic fracture propagation in tight oil reservoirs by volumetric fracturing. *Pet. Sci.* **2015**, *12*, 674–682. [[CrossRef](#)]
55. Zeng, Q.; Yao, J.; Shao, J. An extended finite element solution for hydraulic fracturing with thermo-hydro-elastic-plastic coupling. *Comput. Method Appl. Mech. Eng.* **2020**, *364*, 1129–1167. [[CrossRef](#)]
56. Ouchi, H.; Katiyar, A.; York, J.; Foster, J.T.; Sharma, M.M. A fully coupled porous flow and geomechanics model for fluid driven cracks: A peridynamics approach. *Comput. Geotech.* **2015**, *55*, 561–576. [[CrossRef](#)]
57. Crouch, S.L.; Starfield, A.M. *Boundary Element Methods in Solid Mechanics*; George Allen & Unwin: London, UK, 1983.
58. Sneddon, I.N.; Elliott, H.A. The opening of a Griffith crack under internal pressure. *Q. Appl. Math.* **1946**, *4*, 262–267. [[CrossRef](#)]

Disclaimer/Publisher’s Note: The statements, opinions and data contained in all publications are solely those of the individual author(s) and contributor(s) and not of MDPI and/or the editor(s). MDPI and/or the editor(s) disclaim responsibility for any injury to people or property resulting from any ideas, methods, instructions or products referred to in the content.